

pubs.acs.org/JPCC Article

# Switching a Plasmon-Driven Reaction Mechanism from Charge Transfer to Adsorbate Electronic Excitation Using Surface Ligands

Hamed Kookhaee, Tefera E. Tesema, and Terefe G. Habteyes\*



Cite This: J. Phys. Chem. C 2020, 124, 22711–22720



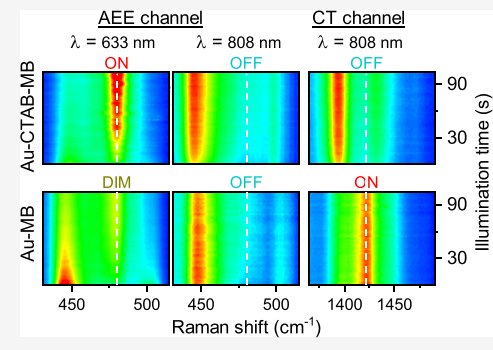
**ACCESS** 

Metrics & More

Article Recommendations

Supporting Information

**ABSTRACT:** Understanding photocatalytic reaction conditions that selectively leads to a desired product on metal surfaces is a longstanding research problem in heterogeneous catalysis. Here, using plasmon-enhanced *N*-demethylation of methylene blue (MB) as model reaction, we show that a high degree of product selectivity can be achieved by switching the mechanism from charge transfer (CT) to adsorbate electronic excitation (AEE). In the presence of a cetyl trimethyl ammonium bromide (CTAB) surface ligand on gold nanoparticles, MB is selectively transformed to thionine at a 633 nm excitation wavelength that overlaps with the electronic transition of the adsorbate. The AEE mechanism involves near-field-enhanced intramolecular electronic excitation of the MB adsorbate, and this mechanism is favored by the presence of CTAB that appears to increase the rate of adsorbate excitation by orienting the molecular dipole along the driving surface



field and to prolong the lifetime of the excited state by slowing down adsorbate-to-metal energy transfer. On the other hand, when MB is directly adsorbed on the nanoparticles, the mechanism involves electron transfer that may lead to the formation of an anionic complex. In situ surface-enhanced Raman scattering spectra suggest that the complex remains stable at long excitation wavelengths (808 and 785 nm), while at shorter wavelengths (671, 633, and 561 nm), it may undergo nonselective *N*-demethylation, yielding partially demethylated derivatives in addition to thionine. These experimental observations underscore the importance of adsorption condition in determining the mechanism of plasmon-enhanced photocatalytic reactions.

## 1. INTRODUCTION

The making and breaking of chemical bonds at adsorbatemetal interfaces using light energy has long been the subject of extensive fundamental research interest because of its prospect in important applications including solar energy conversion to chemical fuels and decontamination of chemical exhausts. In general, the mechanism of photochemistry on metal surfaces is discussed in terms of electronic excitation of the adsorbate or adsorbate-metal complex, hot-charge-carrier generation in the metal and transfer to the adsorbate, and thermal effects that follow photoexcitations. In the proximity of the metal surface, the electronic structure and bond energies in the adsorbate can be altered significantly compared to that in the gas phase. The surface-induced perturbation on the properties of the adsorbate combined with the possible involvement of charge carriers and thermal effects in the reaction pose a grand challenge to clearly understand the mechanism of photochemistry on metal surfaces.

Excitation of localized surface plasmon resonances (collective oscillation of conductive electrons coupled to light) provides a dual opportunity to initiate and probe the surface chemistry in situ and reveal new insights that may not be obtained from any other techniques.<sup>2</sup> Examples of plasmondriven chemical reactions include O<sub>2</sub> dissociation,<sup>3</sup> H<sub>2</sub> dissociation,<sup>4</sup> azo-coupling of self-assembled *para*-aminothiophenol<sup>5-11</sup> and *para*-nitrothiophenol,<sup>12-17</sup> esterification

of aldehydes, 18 CO<sub>2</sub> hydrogenation, 19 N-demethylation of methylene blue, 20,21 dissociation of dimethyl disulfide, 22 ammonia dissociation, 23 and decomposition of iodonium salts<sup>24</sup> (see recent reviews<sup>25–27</sup>). Some of the experimental observations, for example, the conversion of CO<sub>2</sub> to CH<sub>4</sub>, indicate that plasmon-enhanced photocatalysis can be optimized to achieve product selectivity. However, despite increasing reports of experimental observations and the prospect of product selectivity, the mechanism of plasmonenhanced photochemistry remains a subject of vigorous debate, particularly on the importance of hot electron transfer versus thermal effects. 23,27-32 The mechanism is debated mainly based on the dissociation reactions of small molecules that include H<sub>2</sub>, O<sub>2</sub>, CO<sub>2</sub>, and NH<sub>3</sub>. For these molecules, the molecule-metal interaction is complex that results in strong perturbation of the electronic structures of the adsorbates with respect to gas-phase properties.33-35 In these types of molecule-metal complexes, separating the contribution of

Received: August 15, 2020 Revised: September 23, 2020 Published: September 24, 2020



charge carriers and thermal effects can be difficult. <sup>27,29,36</sup> In addition, the importance of direct electronic excitation of adsorbates or the adsorbate-metal complex cannot be ruled out as the interaction can shift and create quantum states such that electronic transition from the highest occupied molecular orbital (HOMO) to the lowest unoccupied molecular orbital (LUMO) is accessible even in the visible spectral region.

Clarity into the mechanism of plasmon-driven photochemistry on metal nanoparticles can be obtained using model molecular systems that show minimal geometrical distortion up on adsorption. In particular, the fundamental importance of adsorbate electronic excitation (AEE) in plasmon-enhanced photochemistry can be demonstrated unambiguously using organic molecules that interact with the metal surface through weak van der Waals interactions<sup>37,38</sup> as model systems. Methylene blue (MB), which is a family of organic dyes with a  $\pi$ -conjugated-fused aromatic ring, has such characteristics with a known electronic absorption band of the adsorbate on gold.<sup>39</sup> It has been reported that, in the presence of oxygen and water, MB undergoes plasmon-enhanced Ndemethylation under resonant excitation, that is, when the excitation energy matches the HOMO-LUMO transition energy. 20,21 On the other hand, elimination of benzyl and ethyl groups from viologen derivatives has been observed on gold nanostructures at an excitation wavelength (785 nm) that does not overlap with the electronic absorption bands of the reactants, indicating the importance of the electron transfer mechanism in the plasmon-driven breaking of the C-N bond. 40 However, the experimental conditions that lead to either AEE or charge transfer (CT) mechanisms remain unknown.

In this work, using plasmon-enhanced N-demethylation of MB as model reaction, we show that the mechanism can be switched from CT to AEE depending on the adsorption condition and excitation wavelengths. This is confirmed by recording the vibrational signatures of different N-demethylation derivatives as they form using surface-enhanced Raman scattering (SERS) spectroscopy at five different laser wavelengths (808, 785, 671, 633, and 561 nm). The observation of different species is attributed to different reaction mechanisms. When MB is directly adsorbed on the metal surface, the CT mechanism appears to lead to the formation of the anionic complex that undergoes nonselective N-demethylation reaction at 671, 633, and 561 nm but remains stable at 808 and 785 nm. On the other hand, in the presence of CTAB as coadsorbate, the AEE mechanism leads to the formation of thionine, a complete N-demethylation product. The AEE mechanism involves the following steps: the HOMO-LUMO  $(S_0 \rightarrow S_1)$ transition of MB, the singlet-triplet  $(S_1-T_1)$  intersystem crossing through the spin-vibronic mechanism, and energy transfer from the T1 state to molecular oxygen to generate singlet oxygen that triggers the N-demethylation reaction. 2,20,21 We propose that the presence of CTAB favors the AEE mechanism by orienting the molecular dipole along the driving surface field and increasing the rate of the  $S_0 \rightarrow S_1$  transition as well as by prolonging the excited-state lifetime and slowing down adsorbate-to-metal energy transfer.

#### 2. METHODS

**2.1. Sample Preparation.** Aqueous solutions of gold nanorods (~40 nm diameter and ~80 nm length) with a CTAB surface ligand and gold nanospheres (~50 nm diameter) with a carboxylic acid (CA) surface ligand were

obtained from Nanopartz, Inc. Methylene blue solid powder ( $C_{16}H_{18}ClN_3S\cdot xH_2O$ ) was obtained from Sigma-Aldrich. The excess stabilizing surfactant was removed through two rounds of centrifugation (at 5000 rpm for 5 min) of diluted colloidal solution (0.5 mL is diluted to 1.5 mL in ultrapure water), removing the supernatant at each step. Solid residues of the nanoparticles were then resuspended in freshly prepared 2  $\times$   $10^{-5}$  M MB solution in ultrapure water overnight (~8 h) to ensure the adsorption of MB on the surface of the nanoparticles. The MB/nanoparticle solution was centrifuged, and the supernatant solution was disposed so that the nonadsorbed MB molecules are removed. The solid residue was then resuspended in 100  $\mu$ L of ultrapure water. The final solution was drop-casted on a silicon substrate and dried in an ambient atmosphere.

To rule out the effect of different crystallinities of the gold nanorods and gold nanospheres on the photochemistry, surface ligand exchange is performed as follows: (1) Solid residues of gold nanorods were obtained through the procedures described above. (2) Solution of the CA surfactant was obtained by centrifuging the gold nanosphere solution and taking the supernatant carefully. The gold nanorod solid residue obtained in (1) is then resuspended in the solution of CA obtained in (2).

Plasmonic nanostructures without surface ligands were prepared through deposition of gold of nominal thickness 6 nm on a silicon wafer using electron beam evaporation. This procedure creates gold nanoislands with broad plasmon resonance in the visible and near-infrared regions. Adsorption of MB was achieved by immersing the substrate with the gold nanoislands in freshly prepared  $2\times 10^{-5}$  M MB solution overnight. The substrate pulled out of the solution was dried by blowing with nitrogen gas immediately.

2.2. SERS and Atomic Force Microscope (AFM) Analysis. The SERS measurements were carried out using the AFM/near-filed microscope platform of Neaspec GmbH. The samples were illuminated at excitation wavelengths of  $\lambda$  = 808, 785, 671,633, and 561 nm with about a 1.0 mW incident laser power (P). The laser beam was focused on the sample by using a parabolic mirror (0.46 numerical aperture, NA) at a 60° angle of incidence (with respect to surface normal). Because of the grazing incidence, the focus spot on the sample has an elliptical shape with diameters d and 2d. Approximating d from the diffraction limit relation, the laser intensity can be estimated as  $0.54P/\lambda^2$ , which gives  $0.8 \text{ mW/}\mu\text{m}^2$  at 808 nm and 1.7 mW/ $\mu$ m<sup>2</sup> at 561 nm. The scattered light was collected by the same parabolic mirror, directed to the opposite direction (see Figure S1), and focused on the slit of the spectrometer (IsoPlane Spectrograph of Princeton Instruments) that uses a thermoelectrically cooled (-75 °C) and back-illuminated deep depletion CCD camera. On each sample, SERS spectra from at least 10 different locations are recorded, and the average spectra are considered in our analysis.

**2.3. Dark-Field Scattering Spectroscopy.** The plasmon resonances of the gold nanoparticles assembled on the substrate are determined by dark-field scattering spectroscopy using the GX51 Olympus microscope along with the spectrometer mentioned above. The sample is excited with a 100 W halogen white light source using a dark-field microscope objective (MPLFLN100XBD, Olympus) with 0.9 NA. Dark-field images of the nanoparticles are obtained by directing 10% of the signal to the camera (Olympus UC30)

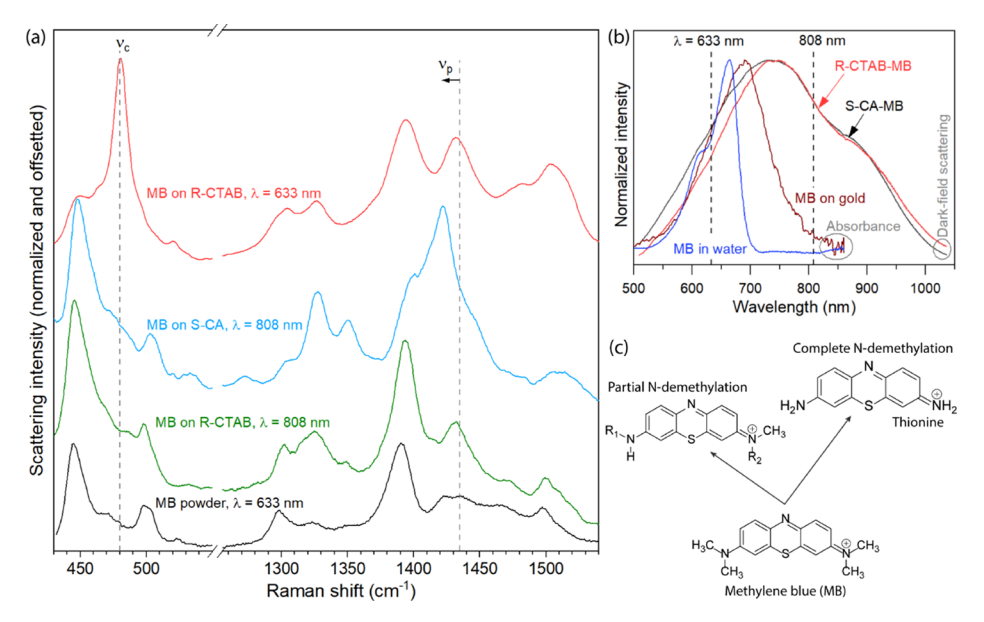


Figure 1. Wavelength and surface ligand-dependent selectivity of plasmon-driven reaction. (a) Representative SERS spectra recorded at 103 s of illumination of MB on gold nanorods with the CTAB surface ligand (R-CTAB) at  $\lambda = 808$  nm (olive line), on gold nanospheres with the carboxylic acid surface ligand (S-CA) at  $\lambda = 808$  nm (blue line), and on R-CTAB at  $\lambda = 633$  nm (red line). The normal Raman spectrum of MB powder (black line) is included as a reference. (b) Absorption spectra of MB in water (blue line), on gold (brown line), and dark-field scattering spectra of R-CTAB with MB adsorbate (red line) and S-CA with MB adsorbate (black line). The 633 nm excitation wavelength overlaps with both the MB absorption band and plasmon resonance (scattering spectra), while 808 nm overlaps only with the plasmon resonance. (c) Proposed photochemical reactions. The possible partial *N*-demethylation products are azure B ( $R_1 \equiv R_2 = CH_3$ ), azure A ( $R_1 = H$ ,  $R_2 = CH_3$ ), azure S ( $R_1 = CH_3$ ,  $R_2 = H$ ), or azure C ( $R_1 \equiv R_2 = H$ ).

attached to the microscope, and representative spectra are recorded by directing 90% of the signal to the spectrometer.

**2.4. Scanning Electron Microscope.** High-resolution structural characterization of samples is carried out using a scanning electron microscope (Quanta 3D FEG).

# 3. RESULTS AND DISCUSSION

The representative SERS spectra in Figure 1a show that the vibrational signatures observed for MB adsorbed on gold nanospheres with a carboxylic acid surface ligand (S-CA) at  $\lambda$ = 808 nm (blue line) is starkly different from that obtained for the MB adsorbed on gold nanorods with the CTAB surface ligand (R-CTAB) at  $\lambda = 633$  nm (red line). Both spectra exhibit new peaks that may be attributed to different degrees of photochemical N-demethylation of MB<sup>20,41</sup> and formation of an anionic complex resulting from metal to molecule electron transfer. At the 633 nm excitation of MB on R-CTAB, the spectrum is dominated by a strong peak at 479 cm<sup>-1</sup>, which is due to the skeletal deformation vibration mode of the thionine product.<sup>21</sup> For MB adsorbed on R-CTAB, the SERS spectra obtained at 808 nm is in very good agreement with the normal Raman spectra of MB solid powder (black line in Figure 1a), indicating that N-demethylation reaction does not take place at the near-infrared excitation wavelength in the presence of CTAB. However, when MB is adsorbed on S-CA, a strong peak appears at ~1422 cm<sup>-1</sup> at an 808 nm excitation even though the 479 cm<sup>-1</sup> peak is absent. This observation indicates the formation of a different species at the 808 nm excitation depending on the adsorption condition. It has been reported that MB can undergo partial N-demethylation (see Figure 1c and Scheme S1) in addition to the complete N-demethylation (thionine formation) indicated by the appearance of the 479 cm<sup>-1</sup> peak (labeled as  $\nu_c$  in Figure 1a).<sup>20</sup> In SERS measurement, the surface-molecule interaction and partial N-

demethylation reaction is indicated by the relative intensity and shifting of the peak labeled  $\nu_{\rm p}$  in Figure 1a. <sup>20</sup>

The stark differences in the reactivity depending on the excitation wavelength and adsorption condition will be explained referring to the overlap of the excitation wavelengths with the MB adsorbate electronic absorption band, which is within the broad band of the plasmon resonances of the nanoparticle aggregates (Figure 1b). The dark-field spectra in Figure 1b show that the resonances of the aggregates are significantly broadened and red-shifted compared to the absorption spectra of the colloidal solution presented in Figure S2. Because of this broadening, the plasmon resonances overlap with all the lasers in our experiments. We note that the plasmon resonances of individual gold nanospheres have a much faster dephasing time than gold nanorods mainly because their resonances peak around 530 nm (Figures S2c) at which the material loss due to interband transition is strong.<sup>42</sup> However, for the aggregates, the resonances are shifted to the red, and the material loss becomes less important.

To obtain insights into the different mechanisms depending on the excitation wavelength and surface ligands, the temporal evolution of the SERS spectra for MB adsorbed on R-CTAB and S-CA is compared at five different excitation wavelengths. The intensity map in Figure 2a,b shows the changes within 103 s in the spectral region that includes the 479 cm<sup>-1</sup> band that indicates the conversion of MB to thionine, while the intensity map in Figure 2d,e shows the changes in the 1422–1435 cm<sup>-1</sup> region due to charge transfer and formation of partial *N*-demethylation (PND) derivatives. The plots in Figure 2c,f are the last spectra in the intensity map after they are normalized to the same maxima to facilitate the comparison of the relative intensities. The full spectra obtained at 0.5 and 103 s of illumination are provided in Figures S4a,b.

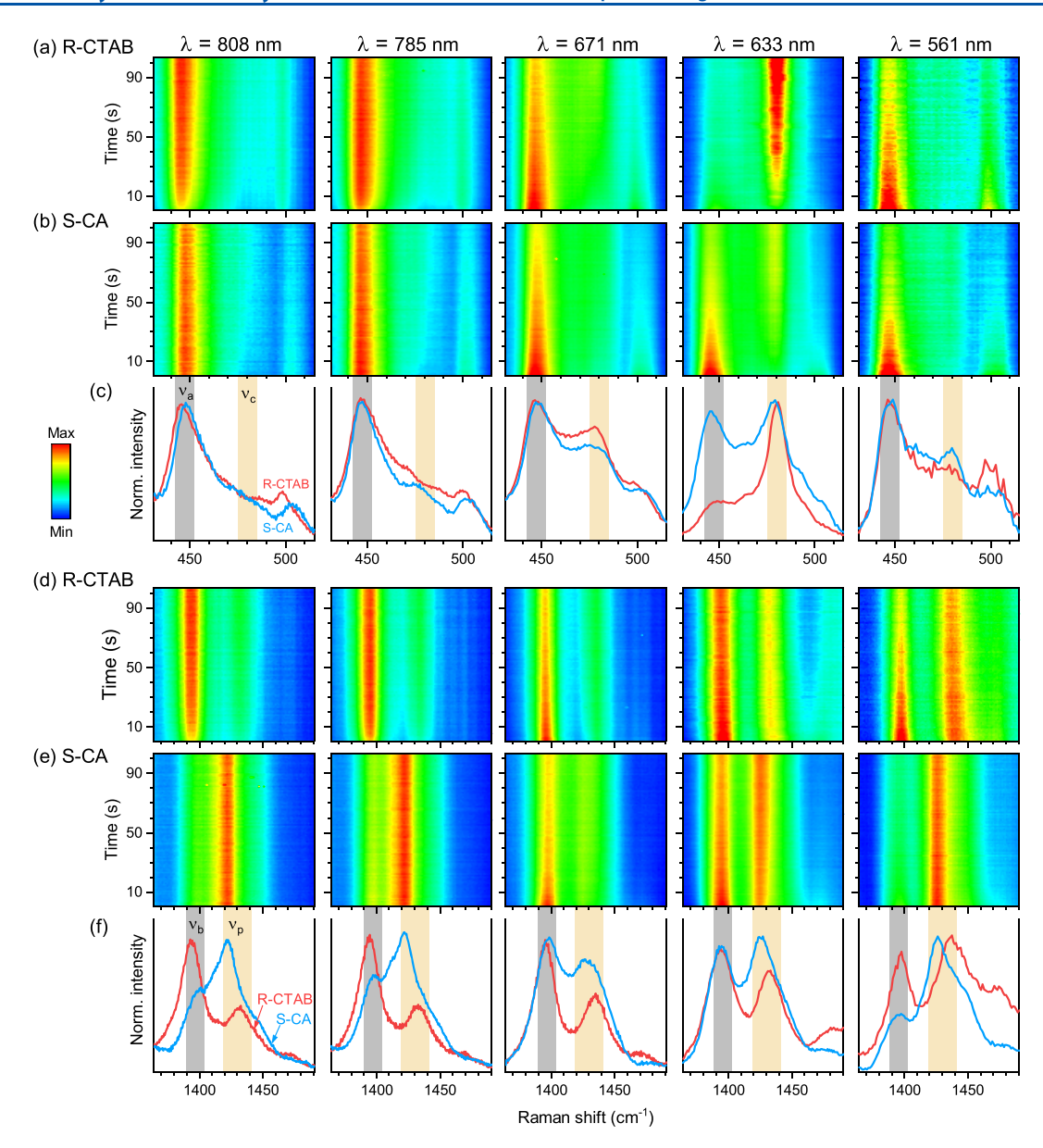


Figure 2. Intensity map of SERS spectra showing the temporal evolution at different excitation wavelengths. (a, b) Intensity map of the 430–515 cm<sup>-1</sup> spectral region for MB adsorbed on R-CTAB (a) and on S-CA (b). (c) The last spectra out of 200 spectra included in the intensity map are shown by the red line (MB on R-CTAB) and blue line (MB on S-CA). The spectra are normalized to the same maximum. The peak labeled  $\nu_c$  indicates the formation of thionine due to complete N-demethylation of MB. The peak labeled  $\nu_a$  is used as a reference. (d, e) Same as (a)–(c) for the spectral region of 1364–1490 cm<sup>-1</sup> that shows the shifting of the band at 1435 cm<sup>-1</sup> toward 1422 cm<sup>-1</sup> due to formation of PND products or charge transfer process. The relative intensity and peak position of the mode labeled  $\nu_p$  indicate partial N-demethylation and/or charge transfer, which will be analyzed with reference to the peak labeled  $\nu_b$ .

**3.1.** Adsorbate Electronic Excitation and Transformation of MB to Thionine. As mentioned above, the extent of MB-to-thionine conversion as a function of time can be assessed by comparing the  $\nu_c$  band intensity to the intensity of the band at ~446 cm<sup>-1</sup> (labeled  $\nu_a$  in Figure 2c) that does not exist in the thionine spectrum. Except at  $\lambda = 633$  nm, the relative intensity of the  $\nu_a$  peak is significantly higher than that of  $\nu_c$  throughout the illumination time as can be seen in the intensity maps. In addition, comparison of the relative intensities at  $\lambda = 633$  nm (Figure 2a,b) indicates that the  $\nu_c$  band intensity is significantly stronger when MB is adsorbed on R-CTAB than on S-CA. The dependence of the reaction on the excitation wavelength and surface ligand is further illustrated by plotting the  $\nu_c/\nu_a$  peak intensity ratio as a

function of time and is shown in Figure 3a,b. For MB on R-CTAB at 633 nm, the  $\nu_{\rm c}/\nu_{\rm a}$  ratio increases from 0.8 to 3.6 as the illumination time increases from 0.5 s to about 103 s, whereas the ratio is smaller than 0.8 at 671 nm and smaller than 0.5 at the other excitation wavelengths during the illumination. On S-CA at 633 nm, the ratio increases from 0.3 to 1.1 and from 0.18 to 0.25 at 808 nm as the illumination time increases from 0.5 to 103 s. This observation indicates that both the excitation wavelength and surface ligand have a remarkable effect on the photochemical transformation of MB to thionine. We note that the fact that the  $\nu_{\rm c}/\nu_{\rm a}$  at 633 nm for the first spectra is significantly larger than that obtained at other wavelengths indicates the formation of thionine within 0.5 s, the acquisition time of each spectrum.

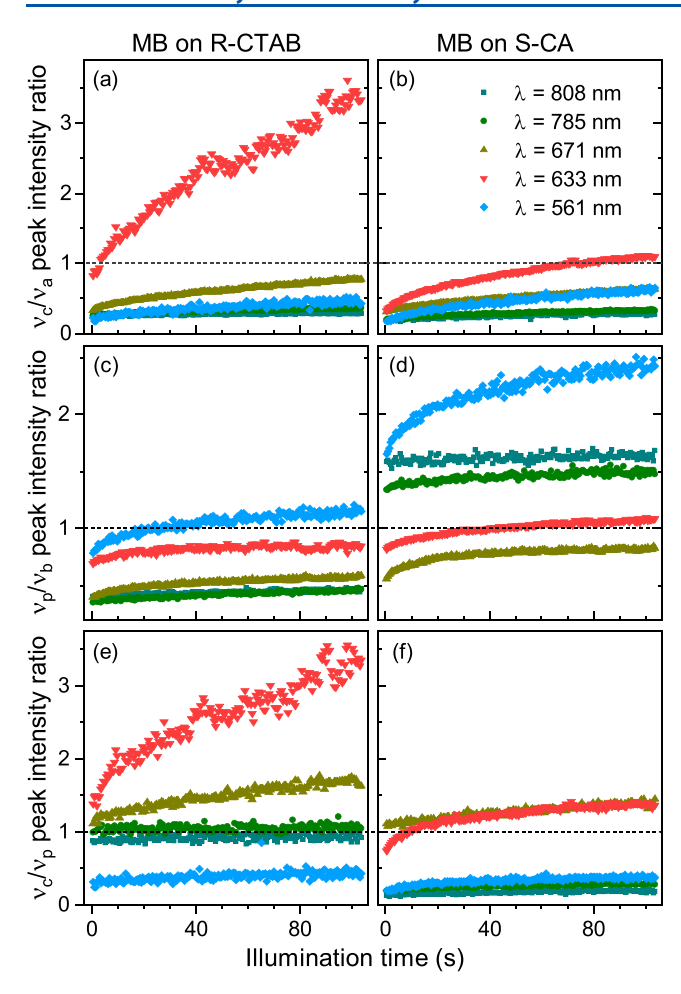
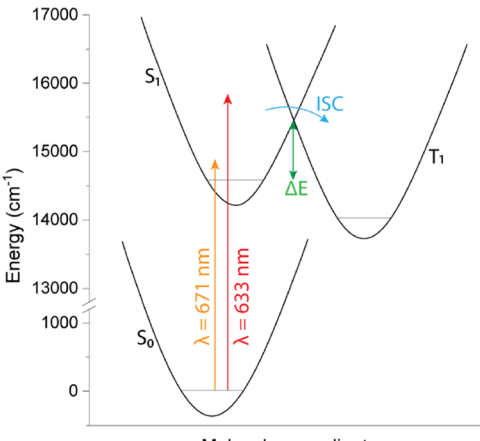


Figure 3. Peak intensities of N-demethylation products with respect to the corresponding reference peaks. Relative peak intensities of (a, b) thionine  $(\nu_c/\nu_b)$  and (c, d) PND product and/or charge transfer  $(\nu_p/\nu_b)$  for MB adsorbed on R-CTAB (a, c) and on S-CA (b, d). (e, f) Thionine-to-PND product intensity ratio  $(\nu_c/\nu_p)$  for MB adsorbed on R-CTAB (e) and S-CA (f) that indicate product selectivity. A ratio larger than 1.0 (dotted horizontal line) indicates selectivity toward thionine (complete N-demethylation), a ratio smaller than 1.0 indicates selectivity toward PND and/or charge transfer, and a ratio close to 1.0 indicates nonselective or no reaction.

The fact that the photochemical transformation of MB to thionine is most effective at the 633 nm excitation wavelength is attributed to excitation of the  $S_0 \rightarrow S_1$  electronic transition in MB that leads to  $S_1$ - $T_1$  intersystem crossing (ISC) and is illustrated in Figure 4. In Figure 4, the values on the y-axis are derived from the absorption spectrum (Figure S3b), and the curves are schematic drawn in the spirit of the discussion in ref 43. As can be seen in Figure 1b and Figure S3b, the 671 nm excitation wavelength is closer to the absorption peak (0-0 transition), whereas the 633 nm overlaps with the shoulder peak (0-1 transition)<sup>44</sup> and is illustrated in Figure S3. This observation may suggest that the ISC involves spin-vibronic mechanisms. 43 At 671 nm, the population of excited vibrational states in the S1 state is expected to be low, and hence, crossing over the energy barrier ( $\Delta E$ ) will be unlikely. At 633 nm, the density of excited vibrational states in the S<sub>1</sub> state can be sufficiently large, and ISC can take place at ultrafast speed through motion along certain vibrational degrees of freedom. <sup>43</sup> Once the triplet state is prepared, the MB  $(T_1)$  to  $O_2$   $(X^3\Sigma_g^-)$ , ground state) energy transfer can lead



Molecular coordinate

**Figure 4.** Schematic showing electronic transition and intersystem crossing (ISC) in MB. The energy scale is derived from the absorption spectrum of the adsorbate (Figure S3). At 671 and 633 nm, the transitions may primarily be characterized as 0-0 and 0-1, respectively. Note that the two transitions are barely resolved in the absorption spectra, which indicates a large number of normal modes (density of vibrational states in each electronic state) as manifested in the SERS spectra of MB.  $\Delta E$  on the plot indicates the barrier energy for crossing from the singlet-excited state  $(S_1)$  to the triplet-excited state  $(T_1)$ .

to generation of singlet oxygen that triggers the N-demethylation reaction as described in our recent report.  $^{20}$ 

3.2. Charge Transfer and PND at Off-Resonance **Excitation Wavelengths.** The results in Figure 2d,e show that the relative intensities of the bands depend on the excitation wavelength and adsorption condition. For MB on R-CTAB at 808 and 785 nm excitation wavelengths that do not have significant overlap with the electronic absorption band of MB (Figure 1b), the spectra are characteristic of MB Raman spectra that is dominated by the vibrational band in the gray region labeled as  $\nu_{\rm b}$  in Figure 2f. For MB on R-CTAB, the relative intensity of the  $\nu_{\rm p}$  vibrational band becomes dominant only at the shortest wavelength (561 nm) and can be seen in Figure 2f. The spectral pattern is drastically different for MB on S-CA particularly at 808 and 785 nm excitation wavelengths at which the dominant band is centered at  $\nu_p \sim 1422 \text{ cm}^{-1}$ , while the  $\nu_{\rm b}$  mode appears as a shoulder (see the blue lines in Figure 2f). At 671 and 633 nm that overlap with the electronic transition of the MB adsorbate, the relative intensity of the  $\nu_{\rm p}$ band is comparable to that of the  $\nu_{\rm b}$  band and becomes dominant again at 561 nm. In addition to the relative intensity, the peak position of the  $\nu_{\rm p}$  band varies depending on the excitation wavelength and adsorption condition.

The variation of the spectral patterns depending on the excitation wavelength and adsorption conditions can be attributed partly to the photochemical transformation of MB to different PND derivatives. Comparison of the normal Raman and corresponding SERS spectra acquired in an inert atmosphere indicate that the relative intensity of the  $\nu_{\rm p}$  band increases and its peak position shifts to the red if MB is converted to azure B and azure A<sup>20</sup> (see also Figure S5). Based on this background information, it is clear that the formation of PND derivatives is more favorable when MB is adsorbed on S-CA (blue lines) than on R-CTAB (red lines). As shown in Figure 5, for MB adsorbed on R-CTAB, the  $\nu_{\rm p}$  mode frequency red shift ranges from negligible at 808 nm to  $\sim$ 6 cm<sup>-1</sup> at 561 nm. On the other hand, for MB adsorbed on S-CA, the

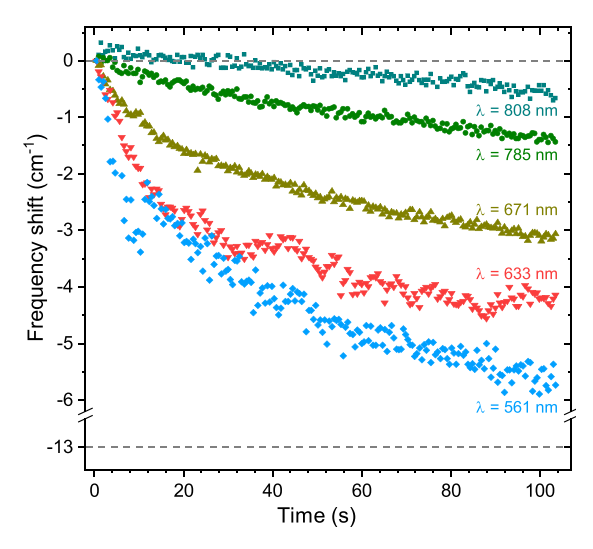


Figure 5. Red-shifting of the  $\nu_{\rm p}$  peak due to partial N-demethylation and/or charge transfer. The horizontal dashed line indicates the maximum shift observed on S-CA at off-resonance excitation wavelengths (808, 785, and 561 nm). The relatively small shift for MB adsorbed on R-CTAB indicates the small extent of partial N-demethylation.

frequency down shift is about 13 cm<sup>-1</sup> (indicated by the dashed horizontal line in Figure 5). We note that comparing the spectral pattern in Figure 2f (blue lines) to that in Figure S5, the extent of the shift and relative intensity increase of the  $\nu_{\rm p}$  band is more significant than expected from the conversion of MB to azure B and azure A, which suggests a dominant contribution of other species.

The conversion of MB to PND products and other species depending on excitation wavelength and adsorption condition can be evaluated using the  $\nu_{\rm b}$  band as a reference. The results in Figure 3c show that on R-CTAB, the  $\nu_{\rm p}/\nu_{\rm b}$  peak intensity ratio is smaller than 1.0 except at  $\lambda=561$  nm at which it increases to  $\sim\!1.2$  at a long illumination time. The wavelength dependence is remarkably different on S-CA (Figure 2e) from that on R-CTAB (Figure 2d). The ratio is larger than 1.0 at excitation wavelengths (808, 785, and 561 nm) that do not have significant overlap with the electronic absorption band of MB adsorbate (Figure 1b). Overall, comparing the results in Figure 3a–d, it is clear that the conditions that favor thionine formation (Figure 3a) are least favorable for the other channel that likely involves electron transfer and vice versa.

To further quantify the product selectivity depending on the excitation wavelength and adsorption conditions, the  $\nu_c/\nu_p$ peak intensity ratios are plotted in Figure 3e,f. On R-CTAB (Figure 3e), the ratio is significantly larger than 1.0 at 633 nm and slightly so at 671 nm, indicating selectivity toward complete N-demethylation (thionine formation); close to 1.0 at 808 and 785 nm, indicating the absence of reaction; and smaller than 0.5 at 561 nm, indicating selectivity toward CTdriven processes. On the other hand, on S-CA, the ratio is smaller than 0.4 at all off-resonance wavelengths (808, 785, and 561 nm), indicating strong selectivity toward CT processes. At 633 and 671 nm, the ratio in Figure 3f increases slightly with an illumination time but only up to about 1.4 compared to 3.6 for MB adsorbed on R-CTAB (Figure 3e), which indicates competing AEE and CT mechanisms depending on the adsorption condition.

**3.3.** Effect of Surface Ligands on Adsorption Geometry and Photochemistry. The results presented in Figures 1–3 demonstrate the observation of preferential photochemical conversion of MB to thionine on R-CTAB, while various chemical species are formed on S-CA due to the CT mechanism, depending on the excitation wavelength. To confirm that the different outcomes of the photochemical reaction is due to the surface ligands but not due to the different crystallinity of the gold nanorods and nanospheres, the SERS measurement is repeated after exchanging the surface ligands, that is, after replacing CTAB with CA on the gold nanorods (see the absorption spectra of the colloidal solution before and after the ligand exchange in Figure S2c,d). The results show that the SERS spectra of MB adsorbed on R-CA (Figure 6b) are different from that obtained by adsorbing on

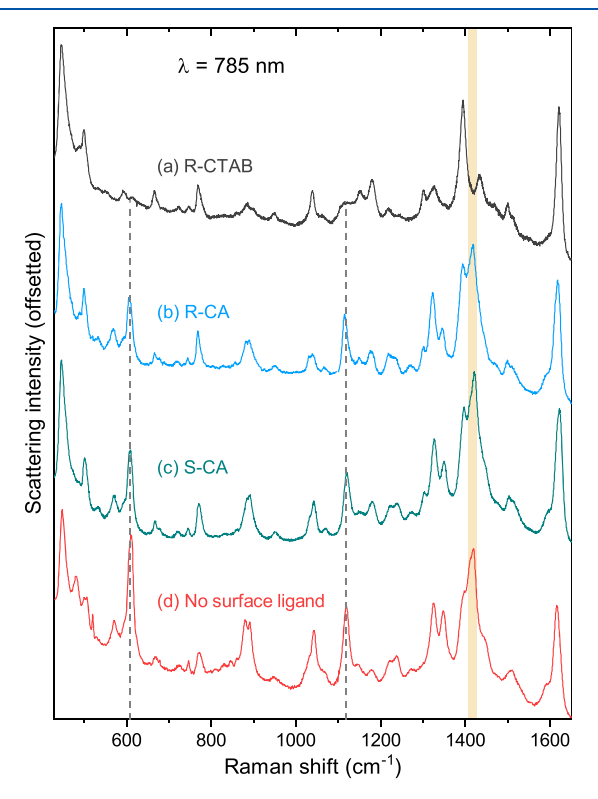


Figure 6. SERS spectra of MB on (a) gold nanorods with the CTAB surface ligand, (b) gold nanorods with the carboxylic acid surface ligand, (c) gold nanosphere with the carboxylic acid surface ligand, and (d) gold nanoislands prepared by electron-beam evaporation (no surface ligand).

R-CTAB (Figure 6a) but similar to the spectra obtained when MB is adsorbed on S-CA (Figure 6c). Interestingly, the spectra obtained by adsorbing MB on the colloidal nanoparticles with the CA surface ligand are in excellent agreement with the spectra obtained when MB is adsorbed on bare gold nanoislands without surface ligands (Figure 6d). Additional results (obtained at 785 and 633 nm) that show the temporal evolution of the SERS spectra of MB on R-CA are presented in Figure S6, and they are in agreement with the corresponding results on S-CA in Figure 2. Therefore, we conclude that, during the solution process that involves incubating the nanoparticles in MB solution, MB replaces CA and adsorbs directly on the gold surface, while CTAB may coadsorb with the analyte molecules.

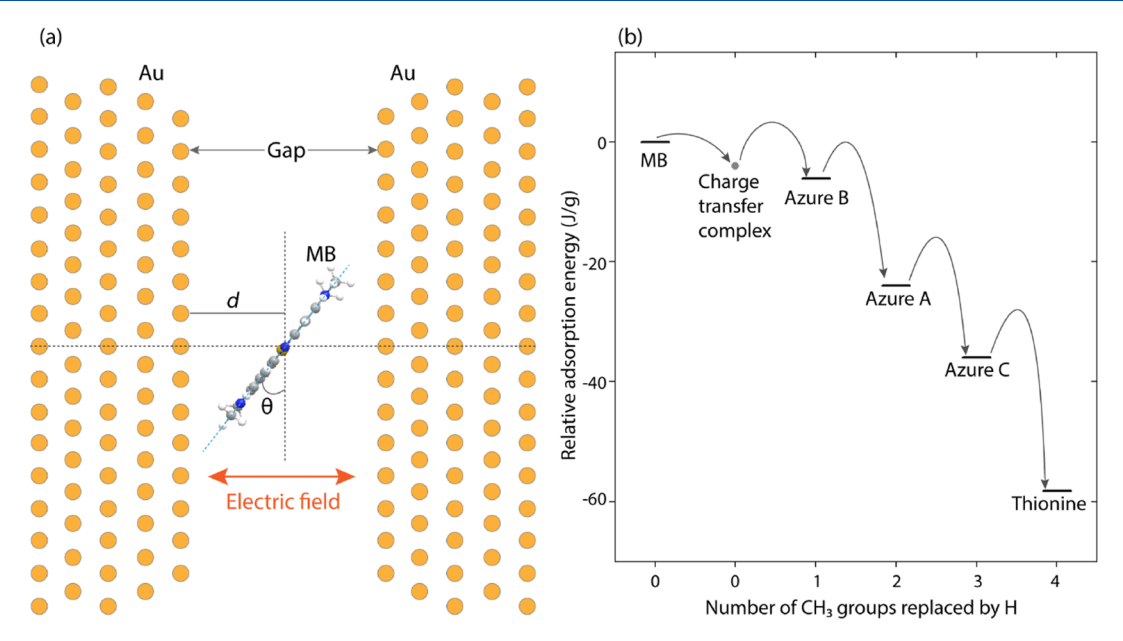


Figure 7. Schematic showing adsorption geometry and energy. (a) The adsorption geometry can vary due to surface ligands that change the orientation angle  $(\theta)$  and surface-molecule separation distance (d). (b) The adsorption energy per unit mass is proposed to increase as the relatively bulky CH<sub>3</sub> group are removed and replaced by hydrogen atom during the *N*-demethylation reaction. The relative adsorption energy is derived from ref. 38 dividing by the corresponding molar mass.

The presence of CTAB coadsorbate can affect the MBsurface separation (d) as proposed in ref 20 and the orientation of MB with respect to the crystal plane  $(\theta)$  as illustrated by the schematic in Figure 7a. The adjustment of d and  $\theta$  in the presence of CTAB can change the outcome of the photochemical reaction. On the bare gold surface, MB is expected to orient parallel to the surface ( $\theta = 0$ ) that favors the  $\pi$ -stacking type of van der Waals interaction with  $d \sim 3.2 \text{ Å.}^{38}$  In our experiment, the nanoparticles are aggregated (see Figure S2) and the SERS signal practically originates from molecules at hot spots of the plasmon field, which is well known to be in narrow gaps between the nanoparticles.<sup>45</sup> In addition, real space mapping of near-field distribution shows that the electric field of the gap plasmon mode is along the interconnecting axis. For  $\theta = 0$  (see Figure 7a), the dipole moment of the molecule  $(\mu)$  will be perpendicular to the electric field (E), and electronic excitation of the adsorbate will be ineffective as the interaction energy  $\mu \cdot E \approx 0$ . The presence of CTAB can increase the population of adsorbates with dipole moment projections along the driving field. In addition, the surface ligand can increase the MB-surface separation slightly, thereby slowing down the rate of molecule-to-metal excitation energy transfer. As a result, the excited state lifetime of the adsorbate increases, leading to MB singlet-to-MB triplet intersystem crossing. MB is a well-known photosensitizer, and in the presence of oxygen in the surface-molecule complex, energy transfer from the excited MB triplet state to the oxygen molecule in the triplet ground state can generate singlet oxygen that triggers the conversion of MB to thionine.<sup>20</sup>

When MB is adsorbed directly on the metal surface, the energy transfer to the metal surface reduces the molecular excited-state lifetime. As a result, the singlet oxygen mechanism becomes less likely. The drastically smaller thionine signal in Figure 3b (MB on S-CA) than in Figure 3a (MB on R-CTAB) can be attributed to this competing process. In the absence of surface ligands that modify the adsorption geometry, the photochemical N-demethylation may be initiated by hot

electron transfer to molecular oxygen. Some insights into this possibility can be obtained from close observation of the wavelength-dependent spectral features.

Theoretically, four products of PND can be formed depending on the extent and atomic site of the Ndemethylation (see Figure 1c and Scheme S1). Comparison of the full spectra (Figure S4a,b) indicates that different species are produced at short (561 nm) and long (808 and 785 nm) excitation wavelengths. Based on the reference spectra provided in Figure S5, it appears that excitation at 561 nm yields mixtures of PND derivatives and possibly other species for MB adsorbed on both R-CTAB and S-CA. On the other hand, illumination of MB adsorbed on S-CA at 808 and 785 nm appears to produce a specific chemical species that is absent during illumination of MB adsorbed on R-CTAB as the results in Figures 2-3 and Figure S4a,b confirm. Comparing the spectra in Figure 6 and Figure S4a,b to the reference spectra in Figure S5, it is clear that the distinct vibrational peaks at 609 and 1121 cm<sup>-1</sup> and the shoulder peak at 1596 cm<sup>-1</sup> cannot be assigned to azure B, azure A, or azure C. On the other hand, the multiple peaks around 804 cm<sup>-1</sup>, which appear in azure A and azure B (Figure S5) and at the 561 nm excitation of MB on S-CA, are completely absent at 808 and 785 nm. Therefore, we conclude that the photochemical process at 808 and 785 nm is highly selective toward the formation of a different chemical species. The fact that the formation of this particular species is effective when MB is directly adsorbed on the metal surface indicates the importance of the surface-molecule interaction and electron transfer processes. This interaction may favor the formation of the derivative that we have labeled as azure S that involves replacing one CH<sub>3</sub> group with hydrogen at each N-terminal. However, it is unlikely that the spectra of azure S will be significantly different from that of the other derivatives considering the structural similarities. In addition, the calculated spectra of azure S (Figure S7b) does not reproduce the experimental observation, while the result of the same

calculation on MB (Figure S7a) is in reasonable agreement with the experimental observation.

The above analysis has forced us to speculate that the spectra observed at 808 and 785 nm excitations for MB directly adsorbed on the gold surface are characteristic of an anionic complex, resulting from metal molecule electron transfer. The complex may be described as S·[MB- $(O_2)_k(H_2O)_mL_n$  where S represents the gold surface, L is the surface ligand, and k, m, are n are integers as it has been proposed recently.<sup>2</sup> We note that the observation of anionic species have been reported recently based on SERS measurements. 47-50 In our experiment, it appears that the charge transfer complex remains stable at the near-infrared wavelengths (808 and 785 nm). On the other hand, vibrational signatures of N-demethylation products are apparent at shorter wavelengths (671, 633, and 561 nm), which may suggest that the anionic complex can undergo N-demethylation reaction. In general, for MB adsorbed directly on gold, the anionic complex may be present at all excitation wavelengths with various degrees of concentrations because of subsequent chemical transformation. Referring to Figure 1b, we can see that the absorption spectrum of MB on gold has the least overlap with the 808 nm wavelength at which the N-demethylation is practically absent. Since the absorption band has some overlaps with the 561 nm wavelength, it may not be possible to conclude with full certainty that N-demethylation can be induced purely by electron transfer without the involvement of electronic excited-state processes. However, it has been proposed that N-demethylation reaction can be initiated by singlet oxygen or a peroxide anion.<sup>51</sup> The reaction can also be assisted by steric effect as the N-demethylation reaction involves replacing the relatively bulky methyl groups with hydrogen atoms. As a result, the molecule-surface interaction becomes favorable as the N-demethylation proceeds and the steric hindrance due to the bulky groups is removed and is illustrated in Figure 7b. We note that the absolute adsorption energy is expected to increase with the molar mass because of the dispersion forces.<sup>38</sup> The results plotted in Figure 7b are taken from ref 38 after normalizing the adsorption energy in ref 38 by the corresponding molar masses, and it shows that the adsorption becomes favorable as the bulky CH3 groups are replaced by H atoms. In addition to the PND derivatives, the stabilization of MB in a charge transfer complex is indicated on the plot in Figure 7b.

3.4. Evidence for the Plasmon-Induced Surface-Molecule Interaction. As it has been discussed so far, illumination of MB adsorbed on R-CTAB at the 808 nm wavelength does not induce N-demethylation of MB as it has been confirmed by the absence of thionine signal (Figures 2a,d, 3a, and S4) and by the negligible frequency shift (Figure 5) of the band that indicates partial N-demethylation. On the other hand, at 808 nm, the vibrational band intensity of MB increases as a function of time and is shown in Figure 2a,d and Figure S8a,c. A similar effect is observed at 785 nm to a lesser extent possibly because of other competing processes such as induced desorption. The relative intensity increase of the SERS signal as a function of time can be attributed to the chemical enhancement effect that increases as the adsorbate molecular coordinates rearrange to create the thermodynamically favorable surface-molecule interaction. 52,53 Adsorbate reorganization is expected to take place at the other excitation wavelengths considered. However, the change in SERS signal due to chemical enhancement effect can be dominated by

other processes that includes plasmon-induced desorption and chemical transformation. The fact that the thionine product signal appears very slowly as a function of the illumination time (see the intensity map of the 479 cm $^{-1}$  band in Figure 2a at 633 nm) suggests adsorbate reorganization before photochemical transformation takes place. Similarly, the magnitude of the  $\nu_{\rm p}$  mode frequency shift that indicates PND product formation increases slowly with time on R-CTAB (Figure 5). On the other hand, on S-CA, the peaks that appear to be characteristic of the anionic complex have a nearly constant peak position and band intensity as a function of the illumination time (Figure 2e), indicating that the charge transfer and coordinate reorganization is much faster than the time needed to acquire the first SERS spectra.

## 4. CONCLUSIONS

In summary, using plasmon-enhanced N-demethylation of methylene blue as model reaction, we have demonstrated that the mechanism of plasmon-driven surface chemical processes can be switched from charge transfer to adsorbate electronic excitation depending on the adsorption of the reactant on the metal nanoparticles. Different products are observed as a result of different mechanisms: the charge transfer mechanism produces the anionic complex and partial N-demethylation products, while the adsorbate electronic excitation leads to the formation of thionine, a complete N-demethylation product. The AEE mechanism involves the following steps: the  $S_0 \rightarrow S_1$ transition of MB,  $S_1$ – $T_1$  intersystem crossing through the spinvibronic mechanism, and energy transfer from the T1 state to molecular oxygen to generate singlet oxygen that triggers the N-demethylation reaction. The AEE mechanism is enhanced by the presence of CTAB coadsorbate that may increase the rate of the  $S_0 \rightarrow S_1$  transition by orienting the molecular dipole along the driving surface field and prolonging the lifetime of excited state by slowing down adsorbate-to-metal energy transfer. The AEE mechanism shows selectivity toward the formation of thionine that involves complete N-demethylation of MB. In contrast, when MB is directly adsorbed on the nanoparticles, signatures of the anionic complex are observed at near-infrared excitation wavelengths, while formation of partial N-demethylation products dominates at shorter wavelengths.

### ASSOCIATED CONTENT

#### Supporting Information

The Supporting Information is available free of charge at https://pubs.acs.org/doi/10.1021/acs.jpcc.0c07479.

Schematic of the experimental setup used to perform the SERS measurement; scanning electron microscope images of methylene blue (MB)-treated gold particles; absorption spectrum of MB in water and adsorbed on gold nanoislands; possible outcomes of MB *N*-demethylation; SERS spectra of MB adsorbed on S-CA and on R-CTAB at different excitation wavelengths at 0.5 and 103 s illumination times; normal and SERS spectra of methylene blue, azure B, azure A, and thionine; intensity map of SERS spectra of MB adsorbed on R-CA; calculated Raman spectra; and change in relative peak intensity of representative modes as a function of illumination time (PDF)

# AUTHOR INFORMATION

#### **Corresponding Author**

Terefe G. Habteyes — Department of Chemistry and Chemical Biology, and Center for High Technology Materials, University of New Mexico, Albuquerque, New Mexico 87131, United States; orcid.org/0000-0001-5978-6464; Email: habteyes@unm.edu

#### **Authors**

Hamed Kookhaee — Department of Chemistry and Chemical Biology, and Center for High Technology Materials, University of New Mexico, Albuquerque, New Mexico 87131, United States; orcid.org/0000-0002-0719-3904

Tefera E. Tesema – Department of Chemistry and Chemical Biology, and Center for High Technology Materials, University of New Mexico, Albuquerque, New Mexico 87131, United States

Complete contact information is available at: https://pubs.acs.org/10.1021/acs.jpcc.0c07479

#### **Author Contributions**

The manuscript was written through contributions of all authors. All authors have given approval to the final version of the manuscript.

#### **Funding**

The U.S. National Science Foundation grant no. 1651478 and the U.S. Air Force Office of Scientific Research grant no. FA9550-18-1-0512.

#### Notes

The authors declare no competing financial interest.

#### ACKNOWLEDGMENTS

This research has been supported by U.S. Air Force Office of Scientific Research (AFOSR), grant no. FA9550-18-1-0512. The Neaspec microscope used for the SERS measurements was upgraded using funding from the U.S. National Science Foundation (NSF) CAREER grant no. 1651478. H.K. was supported by AFOSR Grant. T.E.T. was supported by the NSF grant. T.G.H. received 1 month summer salary from NSF grant and 1 month summer salary from the AFOSR grant during the course of the project. Evaporation of gold was performed at the Center for Integrated Nanotechnologies (CINT), an Office of Science User Facility operated for the U.S. Department of Energy (DOE) Office of Science by Los Alamos National Laboratory (contract DE-AC52-06NA25396) and Sandia National Laboratories (contract DE-NA-0003525).

# ABBREVIATIONS

CTAB, cetyl trimethyl ammonium bromide; CA, carboxylic acid; R-CTAB, gold nanorod with a CTAB surface ligand; S-CA, gold nanosphere with a CA surface ligand; CT, charge transfer; AEE, adsorbate electronic excitation

# **■ REFERENCES**

- (1) Zhou, X.-L.; Zhu, X.-Y.; White, J. M. Photochemistry at Adsorbate Metal Interfaces. Surf. Sci. Rep. 1991, 13, 73–220.
- (2) Tesema, T. E.; Kafle, B.; Habteyes, T. G. Plasmon-Driven Reaction Mechanisms: Hot Electron Transfer Versus Plasmon-Pumped Adsorbate Excitation. *J. Phys. Chem. C* **2019**, *123*, 8469–8483.
- (3) Christopher, P.; Xin, H.; Linic, S. Visible-Light-Enhanced Catalytic Oxidation Reactions on Plasmonic Silver Nanostructures. *Nat. Chem.* **2011**, *3*, 467–472.

- (4) Mukherjee, S.; Libisch, F.; Large, N.; Neumann, O.; Brown, L. V.; Cheng, J.; Lassiter, J. B.; Carter, E. A.; Nordlander, P.; Halas, N. J. Hot Electrons Do the Impossible: Plasmon-Induced Dissociation of H, on Au. *Nano Lett.* **2013**, *13*, 240–247.
- (5) Huang, Y.-F.; Zhu, H.-P.; Liu, G.-K.; Wu, D.-Y.; Ren, B.; Tian, Z.-Q. When the Signal Is Not from the Original Molecule to Be Detected: Chemical Transformation of Para-Aminothiophenol on Ag During the SERS Measurement. J. Am. Chem. Soc. 2010, 132, 9244—9246
- (6) Fang, Y.; Li, Y.; Xu, H.; Sun, M. Ascertaining P,P '-Dimercaptoazobenzene Produced from P-Aminothiophenol by Selective Catalytic Coupling Reaction on Silver Nanoparticles. *Langmuir* **2010**, *26*, 7737–7746.
- (7) Yan, X.; Wang, L.; Tan, X.; Tian, B.; Zhang, J. Surface-Enhanced Raman Spectroscopy Assisted by Radical Capturer for Tracking of Plasmon-Driven Redox Reaction. *Sci. Rep.* **2016**, *6*, 30193.
- (8) Choi, H.-K.; Shon, H. K.; Yu, H.; Lee, T. G.; Kim, Z. H. b<sub>2</sub> Peaks in SERS Spectra of 4-Aminobenzenethiol: A Photochemical Artifact or a Real Chemical Enhancement? *J. Phys. Chem. Lett.* **2013**, *4*, 1079–1086.
- (9) Huang, Y.-F.; Zhang, M.; Zhao, L.-B.; Feng, J.-M.; Wu, D.-Y.; Ren, B.; Tian, Z.-Q. Activation of Oxygen on Gold and Silver Nanoparticles Assisted by Surface Plasmon Resonances. *Angew. Chem.* **2014**, *53*, 2353–2357.
- (10) Zhao, L.-B.; Liu, X.-X.; Zhang, M.; Liu, Z.-F.; Wu, D.-Y.; Tian, Z.-Q. Surface Plasmon Catalytic Aerobic Oxidation of Aromatic Amines in Metal/Molecule/Metal Junctions. *J. Phys. Chem. C* **2016**, 120, 944–955.
- (11) Xu, P.; Kang, L.; Mack, N. H.; Schanze, K. S.; Han, X.; Wang, H.-L. Mechanistic Understanding of Surface Plasmon Assisted Catalysis on a Single Particle: Cyclic Redox of 4-Aminothiophenol. *Sci. Rep.* **2013**, *3*, 2997.
- (12) Dong, B.; Fang, Y.; Xia, L.; Xu, H.; Sun, M. Is 4-Nitrobenzenethiol Converted to P,P '-Dimercaptoazobenzene or 4-Aminothiophenol by Surface Photochemistry Reaction? *J. Raman Spectrosc.* **2011**, 42, 1205–1206.
- (13) Dong, B.; Fang, Y.; Chen, X.; Xu, H.; Sun, M. Substrate-, Wavelength-, and Time-Dependent Plasmon-Assisted Surface Catalysis Reaction of 4-Nitrobenzenethiol Dimerizing to P,P '-Dimercaptoazobenzene on Au, Ag, and Cu Films. *Langmuir* **2011**, 27, 10677—10682.
- (14) Sun, M.; Zhang, Z.; Zheng, H.; Xu, H. In-Situ Plasmon-Driven Chemical Reactions Revealed by High Vacuum Tip-Enhanced Raman Spectroscopy. *Sci. Rep.* **2012**, *2*, 647.
- (15) van Schrojenstein Lantman, E. M.; Deckert-Gaudig, T.; Mank, A. J. G.; Deckert, V.; Weckhuysen, B. M. Catalytic Processes Monitored at the Nanoscale with Tip-Enhanced Raman Spectroscopy. *Nat. Nanotechnol.* **2012**, *7*, 583–586.
- (16) Kang, L.; Xu, P.; Zhang, B.; Tsai, H.; Han, X.; Wang, H.-L. Laser Wavelength- and Power-Dependent Plasmon-Driven Chemical Reactions Monitored Using Single Particle Surface Enhanced Raman Spectroscopy. *Chem. Commun.* **2013**, *49*, 3389–3391.
- (17) Choi, H.-K.; Park, W.-H.; Park, C.-G.; Shin, H.-H.; Lee, K. S.; Kim, Z. H. Metal-Catalyzed Chemical Reaction of Single Molecules Directly Probed by Vibrational Spectroscopy. *J. Am. Chem. Soc.* **2016**, 138, 4673–4684.
- (18) Zhang, Y.; Xiao, Q.; Bao, Y.; Zhang, Y.; Bottle, S.; Sarina, S.; Zhaorigetu, B.; Zhu, H. Direct Photocatalytic Conversion of Aldehydes to Esters Using Supported Gold Nanoparticles under Visible Light Irradiation at Room Temperature. *J. Phys. Chem. C* **2014**, *118*, 19062–19069.
- (19) Zhang, X.; Li, X.; Zhang, D.; Su, N. Q.; Yang, W.; Everitt, H. O.; Liu, J. Product Selectivity in Plasmonic Photocatalysis for Carbon Dioxide Hydrogenation. *Nat. Commun.* **2017**, *8*, 14542.
- (20) Tesema, T. E.; Annesley, C.; Habteyes, T. G. Plasmon-Enhanced Autocatalytic N-Demethylation. *J. Phys. Chem. C* **2018**, 122, 19831–19841.

- (21) Tesema, T. E.; Kafle, B.; Tadesse, M. G.; Habteyes, T. G. Plasmon-Enhanced Resonant Excitation and Demethylation of Methylene Blue. *J. Phys. Chem. C* **2017**, *121*, 7421–7428.
- (22) Kazuma, E.; Jung, J.; Ueba, H.; Trenary, M.; Kim, Y. Real-Space and Real-Time Observation of a Plasmon-Induced Chemical Reaction of a Single Molecule. *Science* **2018**, *360*, 521–526.
- (23) Zhou, L.; Swearer, D. F.; Zhang, C.; Robatjazi, H.; Zhao, H.; Henderson, L.; Dong, L.; Christopher, P.; Carter, E. A.; Nordlander, P.; et al. Quantifying Hot Carrier and Thermal Contributions in Plasmonic Photocatalysis. *Science* **2018**, *362*, *69*–72.
- (24) Miliutina, E.; Guselnikova, O.; Soldatova, N. S.; Bainova, P.; Elashnikov, R.; Fitl, P.; Kurten, T.; Yusubov, M. S.; Švorčík, V.; Valiev, R. R.; Chehimi, M. M.; et al. Can Plasmon Change Reaction Path? Decomposition of Unsymmetrical Iodonium Salts as an Organic Probe. J. Phys. Chem. Lett. 2020, 11, 5770–5776.
- (25) Shin, H.-H.; Koo, J.-J.; Lee, K. S.; Kim, Z. H. Chemical Reactions Driven by Plasmon-Induced Hot Carriers. *Appl. Mater. Today* **2019**, *16*, 112–119.
- (26) Kazuma, E.; Kim, Y. Mechanistic Studies of Plasmon Chemistry on Metal Catalysts. *Angew. Chem., Int. Ed.* **2019**, *58*, 4800–4808.
- (27) Li, X.; Everitt, H. O.; Liu, J. Synergy between Thermal and Nonthermal Effects in Plasmonic Photocatalysis. *Nano Res.* **2020**, *13*, 1268–1280.
- (28) Sivan, Y.; Baraban, J.; Un, I. W.; Dubi, Y. Comment on "Quantifying Hot Carrier and Thermal Contributions in Plasmonic Photocatalysis". *Science* **2019**, *364*, eaaw9367.
- (29) Li, X.; Everitt, H. O.; Liu, J. Confirming Nonthermal Plasmonic Effects Enhance CO<sub>2</sub> Methanation on Rh/TiO<sub>2</sub> Catalysts. *Nano Res.* **2019**, *12*, 1906–1911.
- (30) Dubi, Y.; Sivan, Y. "Hot" Electrons in Metallic Nanostructures-Non-Thermal Carriers or Heating? *Light-Sci. Appl.* **2019**, *8*, 89.
- (31) Jain, P. K. Taking the Heat Off of Plasmonic Chemistry. *J. Phys. Chem. C* **2019**, 123, 24347–24351.
- (32) Sivan, Y.; Baraban, J. H.; Dubi, Y. Experimental Practices Required to Isolate Thermal Effects in Plasmonic Photo-Catalysis: Lessons from Recent Experiments. *OSA Continuum* **2020**, *3*, 483–497.
- (33) Montemore, M. M.; van Spronsen, M. A.; Madix, R. J.; Friend, C. M. O<sub>2</sub> Activation by Metal Surfaces: Implications for Bonding and Reactivity on Heterogeneous Catalysts. *Chem. Rev.* **2018**, *118*, 2816–2862.
- (34) Taifan, W.; Boily, J.-F.; Baltrusaitis, J. Surface Chemistry of Carbon Dioxide Revisited. Surf. Sci. Rep. 2016, 71, 595-671.
- (35) Álvarez, A.; Borges, M.; Corral-Pérez, J. J.; Olcina, J. G.; Hu, L.; Cornu, D.; Huang, R.; Stoian, D.; Urakawa, A. CO<sub>2</sub> Activation over Catalytic Surfaces. *ChemPhysChem* **2017**, *18*, 3135–3141.
- (36) Zhang, X.; Li, X.; Reish, M. E.; Zhang, D.; Su, N. Q.; Gutiérrez, Y.; Moreno, F.; Yang, W.; Everitt, H. O.; Liu, J. Plasmon-Enhanced Catalysis: Distinguishing Thermal and Nonthermal Effects. *Nano Lett.* **2018**, *18*, 1714–1723.
- (37) Ferri, N.; Ambrosetti, A.; Tkatchenko, A. Electronic Charge Rearrangement at Metal/Organic Interfaces Induced by Weak van der Waals Interactions. *Phys. Rev. Mater.* **2017**, *1*, No. 026003.
- (38) Zhou, L.; Johnson, R.; Habteyes, T.; Guo, H. Adsorption of Methylene Blue and Its N-Demethylated Derivatives on the (111) Face of Coinage Metals: The Importance of Dispersion Interactions. *J. Chem. Phys.* **2017**, *146*, 164701.
- (39) Tesema, T. E.; Kookhaee, H.; Habteyes, T. G. Extracting Electronic Transition Bands of Adsorbates from Molecule—Plasmon Excitation Coupling. *J. Phys. Chem. Lett.* **2020**, 3507–3514.
- (40) Brooks, J. L.; Chulhai, D. V.; Yu, Z.; Goodpaster, J. D.; Frontiera, R. R. Plasmon-Driven C-N Bond Cleavage across a Series of Viologen Derivatives. *J. Phys. Chem. C* **2019**, *123*, 29306–29313.
- (41) Kafle, B.; Poveda, M.; Habteyes, T. G. Surface Ligand-Mediated Plasmon-Driven Photochemical Reactions. *J. Phys. Chem. Lett.* **2017**, *8*, 890–894.
- (42) Sönnichsen, C.; Franzl, T.; Wilk, T.; von Plessen, G.; Feldmann, J.; Wilson, O.; Mulvaney, P. Drastic Reduction of Plasmon Damping in Gold Nanorods. *Phys. Rev. Lett.* **2002**, *88*, No. 077402.

- (43) Penfold, T. J.; Gindensperger, E.; Daniel, C.; Marian, C. M. Spin-Vibronic Mechanism for Intersystem Crossing. *Chem. Rev.* **2018**, *118*, 6975–7025.
- (44) Heger, D.; Jirkovský, J.; Klán, P. Aggregation of Methylene Blue in Frozen Aqueous Solutions Studied by Absorption Spectroscopy. *J. Phys. Chem. A* **2005**, *109*, 6702–6709.
- (45) Hao, E.; Schatz, G. C. Electromagnetic Fields around Silver Nanoparticles and Dimers. *J. Chem. Phys.* **2004**, *120*, 357–366.
- (46) Kiesow, K. I.; Dhuey, S.; Habteyes, T. G. Mapping Near-Field Localization in Plasmonic Optical Nanoantennas with 10 nm Spatial Resolution. *Appl. Phys. Lett.* **2014**, *105*, No. 053105.
- (47) Sprague-Klein, E. A.; Negru, B.; Madison, L. R.; Coste, S. C.; Rugg, B. K.; Felts, A. M.; McAnally, M. O.; Banik, M.; Apkarian, V. A.; Wasielewski, M. R.; et al. Photoinduced Plasmon-Driven Chemistry in Trans-1,2-Bis(4-Pyridyl)Ethylene Gold Nanosphere Oligomers. *J. Am. Chem. Soc.* **2018**, *140*, 10583–10592.
- (48) Sprague-Klein, E. A.; McAnally, M. O.; Zhdanov, D. V.; Zrimsek, A. B.; Apkarian, V. A.; Seideman, T.; Schatz, G. C.; Van Duyne, R. P. Observation of Single Molecule Plasmon-Driven Electron Transfer in Isotopically Edited 4,4 '-Bipyridine Gold Nanosphere Oligomers. J. Am. Chem. Soc. 2017, 139, 15212–15221.
- (49) Wang, R.; Li, J.; Rigor, J.; Large, N.; El-Khoury, P. Z.; Rogachev, A. Y.; Kurouski, D. Direct Experimental Evidence of Hot Carrier-Driven Chemical Processes in Tip-Enhanced Raman Spectroscopy (TERS). J. Phys. Chem. C 2020, 124, 2238–2244.
- (50) Wu, Y.; Yang, M.; Ueltschi, T. W.; Mosquera, M. A.; Chen, Z.; Schatz, G. C.; van Duyne, R. P. SERS Study of the Mechanism of Plasmon-Driven Hot Electron Transfer between Gold Nanoparticles and PCBM. J. Phys. Chem. C 2019, 123, 29908–29915.
- (51) Belvedere, A.; Boscá, F.; Cuquerella, M. C.; de Guidi, G.; Miranda, M. A. Photoinduced N-Demethylation of Rufloxacin and Its Methyl Ester under Aerobic Conditions. *Photochem. Photobiol.* **2002**, 76, 252–258.
- (52) Morton, S. M.; Jensen, L. Understanding the Molecule-Surface Chemical Coupling in SERS. J. Am. Chem. Soc. 2009, 131, 4090–4098.
- (53) Valley, N.; Greeneltch, N.; van Duyne, R. P.; Schatz, G. C. A Look at the Origin and Magnitude of the Chemical Contribution to the Enhancement Mechanism of Surface-Enhanced Raman Spectroscopy (SERS): Theory and Experiment. *J. Phys. Chem. Lett.* **2013**, *4*, 2599–2604.